Water wave scattering from a mass loading ice floe of random length using generalised polynomial chaos

J. E. M. Mosig[a,*], F. Montiel[a], V. A. Squire[a]

[a] *Department of Mathematics and Statistics, University of Otago, Dunedin, New Zealand*

Abstract

We consider the scattering of water waves in a two dimensional domain from a floating sea ice floe of random length. The length is treated as a random variable governed by a prescribed probability distribution. To keep the focus on the random length aspect we choose a simple mass loading model to characterise the ice floe. We compute the expectation and variance of the reflection and transmission coefficients using two different methods derived from the framework of generalised polynomial chaos (gPC), as part of which unknown quantities of the problem are expanded in a basis of orthogonal polynomials of the random variable. The polynomials are chosen optimally for the particular probability distribution of the random variable to minimise an approximation error. We devise a stochastic collocation method, which involves computing the reflection and transmission coefficients deterministically for a number of carefully sampled lengths and fitting polynomial expansions to them. The second approach is based on the stochastic Galerkin method, for which the governing equations are transformed to accommodate the random length parameter. We also use a standard Monte Carlo (MC) approach for comparison. The gPC methods are shown to be numerically efficient and exhibit desirable exponential convergence properties, as opposed to the slow inverse square root convergence of the MC approach. Finally, we use the statistic collocation method to demonstrate that the

*Corresponding author

Email addresses: jmosig@maths.otago.ac.nz (J. E. M. Mosig), fmontiel@maths.otago.ac.nz (F. Montiel), vernon.squire@otago.ac.nz (V. A. Squire)

floe size distribution can have a significant impact on the expected transmission coefficient.

Keywords: water wave scattering, random length, generalised polynomial chaos

---

1. Introduction

The scattering of surface gravity waves from compliant floating structures is a well studied problem in ocean engineering and polar geophysics (see e.g. [1]). Floating structures include various man-made objects, such as very large floating structures (VLFSs; see [2]), but also naturally occurring ones, such as sea ice floes [3]. The vast literature on wave scattering by such floating structures has concentrated on characterising (i) the response of the structure to water wave forcing and (ii) the scattered wave field generated from diffraction and radiation processes. The geometry of the structure is typically known or is a function of a number of deterministic parameters, so the method used to solve the scattering problem can be adapted to a certain class of geometries.

Various geometries have been considered in both two and three dimensions. Meylan and Squire [4] devised a Green's function method for the scattering of ocean waves by a floating elastic beam with uniform thickness as a model for a sea ice floe. The same problem was revisited in different fields and solved with a range of numerical methods, such as mode matching [5], integro-differential equations [6] and an integral equation / Galerkin technique [7]. The extension to non-uniform floating beams was considered in [8, 9, 10]. In three dimensions the scattering of water waves by circular elastic plates of uniform thickness was investigated by several authors [11, 12, 13]. Scattering by circular floes with axisymmetric thickness variations was later solved by Bennetts et al. [14] using a multi-mode approximation. Finally, Meylan [15] and Bennetts and Williams [16] developed methods for scattering by elastic plates of arbitrary shape with constant thickness.

It is less clear, however, how uncertainties in the structure's geometry affect the response of the structure and the scattered wave field. This is particularly relevant in the case of sea ice floes, where the general shape varies significantly between individual floes, depending on how they form and then interact with their environment. Taking accurate in situ measurements of the shape and size of individual floes is also challenging [17], so that these properties are usually

given as empirical statistical distributions. To the best of our knowledge no previous studies have attempted to quantify the uncertainty of the scattered wave field due to random variations in the geometry of the structure.

In the present article we conduct a preliminary study to describe the scattering of water waves in two dimensions (one horizontal and one vertical) from an ice floe of random length and uniform thickness. The probability distribution of the length variable is prescribed. We then seek to compute the central moments, i.e. expectation and variance, of the probability distributions of the transmission and reflection coefficients of the ice floe.

Many different methods are available to handle uncertainties in geometry. These include perturbation methods, moment equations, and the Monte Carlo (MC) approach [18]. Perturbation methods, however, typically require perturbations of the parameters and the response of the system to remain small, while the MC approach is known to exhibit slow convergence properties. Here we employ the framework of generalised polynomial chaos (gPC), which does not constrain the size of the random perturbation and converges fast when the system's dependence on the random variables is sufficiently smooth and the number of random variables is small [19].

For problems involving multiple random variables, gPC methods can be problematic as the size of the system of equations arising in such problems increases with the factorial of the random dimension. For example Ganesh and Hawkins [20] found that gPC methods are only practical when the number of random variables is less than 5, but the technique can be extended to a sparse-grid gPC method, which works for more random variables at the expense of reduced accuracy. We also note that, for more complicated problems, such as non-linear wave–body interaction, the quantities of interest may not depend smoothly on the random variable(s), in which case gPC methods would exhibit poor convergence properties. Computationally more intense remedies exist, however, e.g., multi-element gPC methods [21] or wavelet gPC basis functions [22].

The problem considered here involves smooth functions and only a single

random variable (the length of the floe). Consequently, gPC techniques are ideally suited and fast numerical convergence can be expected. The key idea of gPC techniques is to expand the random variable in a basis of mutually orthogonal polynomials. The choice of the polynomial basis is informed by the probability distribution of the random variable. The polynomial expansion provides a spectral representation of the variable in random space, so the scattering problem can be solved using conventional spectral techniques, e.g. mode matching or integral equations.

As the focus of the present work is to introduce the use of gPC methods in a water wave scattering problem, we consider the canonical mass loading model to describe the vertical motion of the ice floe, which does not account for the elasticity of the structure. We acknowledge that the mass loading model is too simple to characterise the motion of an ice floe properly, noting that it has been used by Keller and Weitz [23] to represent pack ice, and later by Wadhams and Holt [24] to represent floating frazil ice. The more standard thin elastic or visco-elastic plate models could be used instead, but this would introduce unnecessary complexity in the implementation of the gPC framework and would not affect the results aimed at demonstrating the efficiency of the framework in a one-dimensional wave scattering problem. The present article also provides the foundation for the extension to three dimensional models where the notion of random length evolves into the notion of random shape. The random boundary of a three dimensional ice floe may then, for example, be described by a Karhunen-Loève expansion in a small number of random variables. Although new issues arise in the three dimensional setting, such as multiple random variables, the basic ideas should carry over in a straightforward manner.

We begin our analysis in §2 with a detailed description of the random floe problem. After briefly discussing the well known fixed length problem in §3, we solve the random length problem using two different gPC methods in §4. Numerical results for both methods are presented in §5 and compared to the MC approach. The focus of the Results section is to demonstrate the attractive convergence properties of the gPC framework for the problem considered here.

As an example, we utilize the good performance of the gPC method to investigate the length-distribution dependence of the expected reflection coefficient of a mass loading floe as a function of floe thickness and wave period. Finally, we conclude with a discussion of our findings in §6.

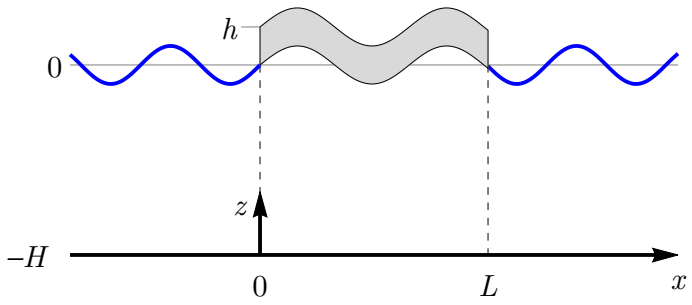

Figure 1: Geometry of the problem.

2. Preliminaries

We consider a two dimensional (one horizontal and one vertical) water domain which is infinitely long horizontally and has finite extent in the vertical direction. In a Cartesian coordinate system (x, z), the vertical dimension is bounded by the equilibrium water surface at $z = 0$ and the flat sea floor at $z = -H$. The water domain is denoted by $\Omega = \{(x, z), -\infty < x < \infty, -H < z < 0\}$. A sea ice floe of thickness h covers the equilibrium water surface between $x = 0$ and $x = L$. For simplicity, we assume the draught of the floe can be neglected. A sketch of the geometry is shown in figure 1.

The water is modelled as an incompressible and inviscid fluid of density $\rho = 1025\,\mathrm{kg\,m^{-3}}$. Further, assuming irrotational and time-harmonic motion, the velocity field of the fluid particles can be expressed as $\mathrm{Re}\{(\partial_x, \partial_z)\phi(x, z)\ \exp(-\mathrm{i}\,\omega\,t)\}$, where ω is the angular frequency and t denotes time. The fluid motion is then fully described by the complex velocity potential $\phi(x, z)$. The time-harmonic condition allows us to replace $\partial_t = -\mathrm{i}\,\omega$ throughout. The incompressibility assumption applied together with mass conservation implies that ϕ satisfies Laplace's equation

$$(\partial_x^2 + \partial_z^2)\phi = 0\ , \qquad \text{for } (x, z) \in \Omega\ . \tag{1}$$

In addition, linearity and conservation of momentum implies that ϕ satisfies the

linearised form of Bernoulli's equation

$$\mathrm{i}\,\omega\,\rho\,\phi = \rho\,g\,z - p\;, \qquad \text{for } (x,z) \in \Omega\;, \tag{2}$$

where $g = 9.8\,\mathrm{m\,s^{-2}}$ is the acceleration due to gravity, and p is the water pressure.

The vertical motion of the ice floe is described by the mass loading model, which corresponds to the Euler-Bernoulli beam equation in the limit of vanishing elasticity. The pressure load $\tilde{p}$ on the beam is then given by

$$\tilde{p} = \omega^2\,\tilde{\rho}\,h\,\eta\;, \tag{3}$$

where $\eta = \eta(x)$ is the surface elevation, h is the thickness of the floe and $\tilde{\rho} = 917\,\mathrm{kg\,m^{-3}}$ is the density of sea ice. Note that the fourth order derivative that appears in the Euler-Bernoulli beam equation [25] is absent in (3). At $z = 0$ the kinematic surface condition holds, i.e.

$$-\mathrm{i}\,\omega\,\eta = \partial_z\phi\;, \qquad z = 0\;. \tag{4}$$

The free surface condition

$$g\,\partial_z\phi = \omega^2\,\phi\;, \qquad z = 0,\ x < 0, x > L\;, \tag{5}$$

follows from (2) and (4). Similarly, assuming $p = -\tilde{p}$ on the bottom surface of the floe and using (2), (4) and (3) yields the mass loading surface condition

$$\left(g - \omega^2\,\rho\,h\right)\partial_z\phi = \omega^2\,\phi\;, \qquad z = 0,\ x \geq 0\;. \tag{6}$$

At the rigid sea floor, the vertical fluid velocity should vanish, i.e.

$$\partial_z\phi = 0\;, \qquad z = -H\;. \tag{7}$$

We prescribe a wave forcing with velocity potential

$$\phi^{\mathrm{In}}(x,z) = A_0\,e^{\mathrm{i}\,\kappa_0\,x}\,\varsigma_0(z)\;, \tag{8}$$

characterising a plane wave travelling in the positive x-direction. The wavenumber κ_0 and vertical function $\varsigma_0(z)$ will be defined in §3. The presence of the ice

floe gives rise to reflected and transmitted wave components, which are given by

$$\phi(x,z) \to \phi^{\mathrm{In}}(x,z) + R\,A_0\,e^{-\mathrm{i}\,\kappa_0\,x}\,\varsigma_0(z)\,, \qquad \text{as } \; x \to -\infty \tag{9}$$

and

$$\phi(x,z) \to T\,A_0\,e^{\mathrm{i}\,\kappa_0\,x}\,\varsigma_0(z)\,, \qquad \text{as } \; x \to \infty\,, \tag{10}$$

respectively, where R and T denote the unknown reflection and transmission coefficients.

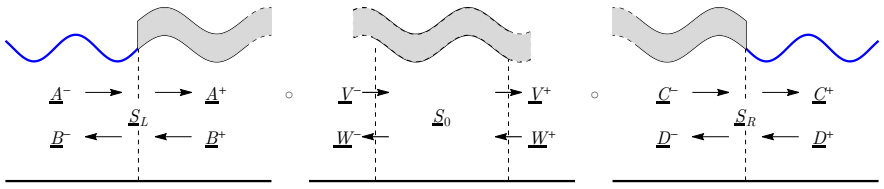

Figure 2: Separation of the deterministic scattering problem into three sub-problems, i.e. scattering from the left edge, phase change of the wave under the floe, and scattering from the right edge.

3. Fixed length scattering

Let us first assume that the length of the ice floe L is a given constant. The scattering problem can be separated into three sub-problems, namely (i) scattering from the left edge, (ii) wave propagation under the floe, and (iii) scattering from the right edge (see figure 2). The solutions of these sub-problems are then combined to describe the scattering by the fixed length ice floe.

3.1. Scattering from the floe edges

We first consider the scattering of waves by the floe's left edge located at $x = 0$. On either side of the edge, we separate variables and represent the solution to Laplace's equation (1) by a plane wave ansatz. Imposing the sea floor condition (7), the free surface condition (5) for $x < 0$ and the mass loading condition (6) for $x \geq 0$, we approximate the potential as truncated series expansions of $N_\zeta + 1$ plane wave modes, i.e.

$$\phi(x,z) \approx \phi^-(x,z) = \sum_{n=0}^{N_\zeta} \left(A_n^- \, e^{\mathrm{i}\,\kappa_n\,x} + B_n^- \, e^{-\mathrm{i}\,\kappa_n\,x} \right) \varsigma_n(z) \,, \qquad x \leq 0 \,, \tag{11}$$

on the left (open water) side of the edge and

$$\phi(x,z) \approx \phi^+(x,z) = \sum_{n=0}^{N_\zeta} \left(A_n^+ \, e^{\mathrm{i}\,k_n\,x} + B_n^+ \, e^{-\mathrm{i}\,k_n\,x} \right) \zeta_n(z) \,, \qquad x \geq 0 \,, \tag{12}$$

on its right (ice-covered) side. We have introduced the vertical modes in the open water and ice-covered domains given by

$$\varsigma_n(z) = \frac{\cosh\left(\kappa_n\,(H+z)\right)}{\cosh\left(\kappa_n\,H\right)} \,, \tag{13}$$

and

$$\zeta_n(z) = \frac{\cosh\left(k_n\left(H+z\right)\right)}{\cosh\left(k_n\,H\right)}\ , \tag{14}$$

respectively. The wavenumbers κ_n and k_n satisfy their respective dispersion relations, i.e.

$$\kappa\,\tanh(\kappa\,H) - \frac{\omega^2}{g} = 0\ , \tag{15}$$

in the open water domain, and

$$k\,\tanh(k\,H) - \frac{\omega^2}{g - h\,\omega^2/\rho} = 0\ , \tag{16}$$

in the ice-covered domain. Both dispersion relations have one real and infinitely many imaginary solutions in the first quadrant of the complex plane. The remaining solutions are the negatives of these and are included in the expansions (11) and (12). The real solutions of (15) and (16) are denoted by κ_0 and k_0, respectively. These solutions are associated with propagating wave modes which do not attenuate with x. We sort the imaginary solutions by increasing magnitude of their imaginary part, i.e. $\mathrm{Im}\{k_{n+1}\} > \mathrm{Im}\{k_n\}$ and $\mathrm{Im}\{\kappa_{n+1}\} > \mathrm{Im}\{\kappa_n\}$, for $n \geq 1$. These correspond to evanescent modes decaying exponentially faster with x as n increases. The truncation of the sums in (11) and (12) at finite N_ζ is therefore justified.

Let the vectors $\underline{A}^- = (A_0^-, \ldots, A_{N_\zeta}^-)^{\mathrm{T}}$ and $\underline{B}^- = (B_0^-, \ldots, B_{N_\zeta}^-)^{\mathrm{T}}$, respectively, contain the complex amplitudes of the right and left propagating modes in the general solution (11). Furthermore, let the vectors $\underline{A}^+ = (A_0^+, \ldots, A_{N_\zeta}^+)^{\mathrm{T}}$ and $\underline{B}^+ = (A_0^+, \ldots, A_{N_\zeta}^+)^{\mathrm{T}}$, respectively, contain the amplitudes of the right and left propagating modes in the general solution (12). By matching the potentials $\phi^- = \phi^+$ and horizontal fluid velocities $\partial_x\phi^- = \partial_x\phi^+$ at the boundary $x = 0$, we can find the following set of relationships describing the reflection and transmission of waves incident on either side of the edge

$$\underline{A}^+ = \underline{T}_L^- \cdot \underline{A}^- + \underline{R}_L^+ \cdot \underline{B}^+\ , \tag{17}$$

$$\underline{B}^- = \underline{R}_L^- \cdot \underline{A}^- + \underline{T}_L^+ \cdot \underline{B}^+\ . \tag{18}$$

where $\underline{T}_L^\pm$ and $\underline{R}_L^\pm$ are matrices of dimension $(N_\zeta+1)\times(N_\zeta+1)$. These matrices are obtained in solving the matching problem numerically. Here, we use an in-

tegral equation method similar to that described in [26] to enforce the matching of potential and normal velocity at $x = 0$, noting that other methods could have been used instead, such as residue calculus techniques [27, 28], an error minimization approach [29], an eigenfunction matching method [30], and variations of these (see [1] for a review). The implementation of the matching procedure is not a focus of the present paper. Only a brief derivation is therefore given in Appendix A. The relationships (17) and (18) can be summarised as

$$\begin{pmatrix} \underline{A}^+ \\ \underline{B}^- \end{pmatrix} = \underline{S}_L \cdot \begin{pmatrix} \underline{A}^- \\ \underline{B}^+ \end{pmatrix} = \begin{pmatrix} \underline{T}_L^- & \underline{R}_L^+ \\ \underline{R}_L^- & \underline{T}_L^+ \end{pmatrix} \cdot \begin{pmatrix} \underline{A}^- \\ \underline{B}^+ \end{pmatrix} . \tag{19}$$

where the matrix $\underline{S}_L$ has dimension $2(N_\zeta + 1) \times 2(N_\zeta + 1)$ and is referred to as the scattering matrix of the left floe edge.

From symmetry considerations, the solution to the right edge scattering problem can be deduced from that of the left edge. Eigenfunction expansions of the potential in the ice-covered and open water regions similar to (11) and (12) can be written down. We introduce the vectors of amplitudes $\underline{C}^- = (C_0^-, \ldots, C_{N_\zeta}^-)^{\mathrm{T}}$ and $\underline{D}^- = (D_0^-, \ldots, D_{N_\zeta}^-)^{\mathrm{T}}$ of the right and left propagating modes, respectively, in the ice-covered region, and analogously $\underline{C}^+ = (C_0^+, \ldots, C_{N_\zeta}^+)^{\mathrm{T}}$ and $\underline{D}^+ = (D_0^+, \ldots, D_{N_\zeta}^+)^{\mathrm{T}}$ for the right and left travelling modes in the open water region. The scattering matrix of the floe's right edge is then defined by

$$\begin{pmatrix} \underline{C}^+ \\ \underline{D}^- \end{pmatrix} = \underline{S}_R \cdot \begin{pmatrix} \underline{C}^- \\ \underline{D}^+ \end{pmatrix} = \begin{pmatrix} \underline{T}_R^- & \underline{R}_R^+ \\ \underline{R}_R^- & \underline{T}_R^+ \end{pmatrix} \cdot \begin{pmatrix} \underline{C}^- \\ \underline{D}^+ \end{pmatrix} . \tag{20}$$

The blocks of $\underline{S}_R$ are related to those of $\underline{S}_L$ by $\underline{T}_R^\pm = \underline{T}_L^\mp$, and $\underline{R}_R^\pm = \underline{R}_L^\mp$.

3.2. Wave propagation in a deterministic domain

We now construct the mapping describing the phase change experienced by the wave modes between the two edges $x = 0$ and $x = L$. Although this is a trivial exercise in the deterministic case, we describe it in detail here to attract the reader's attention to the process as it will be substantially more involved when solving the scattering by a floe of random length in §4.2.

We express the potential under the floe as

$$\phi(x,z) \approx \phi^L(x,z) = \sum_{n=0}^{N_\zeta} \left(V_n^- \, e^{\mathrm{i}\, k_n \, x} + W_n^- \, e^{-\mathrm{i}\, k_n \, x}\right) \zeta_n(z) \; , \qquad x = 0 \; , \tag{21}$$

at its left end, and

$$\phi(x,z) \approx \phi^R(x,z) = \sum_{n=0}^{N_\zeta} \left(V_n^+ \, e^{\mathrm{i}\, k_n \, x} + W_n^+ \, e^{-\mathrm{i}\, k_n \, x}\right) \zeta_n(z) \; , \qquad x = L \; , \tag{22}$$

at its right end. Introducing the vector notations $\underline{V}^\pm = (V_0^\pm, \ldots, V_{N_\zeta}^\pm)^{\mathrm{T}}$, and $\underline{W}^\pm = (W_0^\pm, \ldots, W_{N_\zeta}^\pm)^{\mathrm{T}}$, the propagation process can be summarised by

$$\begin{pmatrix} \underline{V}^+ \\ \underline{W}^- \end{pmatrix} = \underline{S}_0 \cdot \begin{pmatrix} \underline{V}^- \\ \underline{W}^+ \end{pmatrix} \; , \tag{23}$$

where

$$\underline{S}_0 = \begin{pmatrix} \underline{T}_0^- & \underline{R}_0^+ \\ \underline{R}_0^- & \underline{T}_0^+ \end{pmatrix} = \mathrm{diag}(e^{\mathrm{i}\, k_0 \, L}, \ldots, e^{\mathrm{i}\, k_{N_\zeta} \, L}, e^{\mathrm{i}\, k_0 \, L}, \ldots, e^{\mathrm{i}\, k_{N_\zeta} \, L}) \; . \tag{24}$$

The matrix $\boldsymbol{S}_0$ can be regarded as a scattering matrix relating the ingoing and outgoing wave amplitudes.

3.3. Scattering matrix of the fixed length floe

We can now combine the matrices $\underline{S}_L$, $\underline{S}_0$, and $\underline{S}_R$ to obtain the scattering matrix $\underline{S}$ of the mass loading floe.

We begin by combining $\underline{S}_L$ and $\underline{S}_0$, i.e. we seek to compute the matrix $\underline{S}_{L0}$ which relates $\underline{A}^-$ and $\underline{W}^+$ with $\underline{V}^+$ and $\underline{B}^-$. The matrix $\underline{S}_{L0}$ can be found by identifying $\underline{V}^- = \underline{A}^+$ and $\underline{W}^- = \underline{B}^+$, and eliminating $\underline{A}^+$ and $\underline{B}^+$ from the system. We obtain

$$\underline{S}_{L0} = \begin{pmatrix} \underline{T}_{L0}^- & \underline{R}_{L0}^+ \\ \underline{R}_{L0}^- & \underline{T}_{L0}^+ \end{pmatrix} \; . \tag{25}$$

where the blocks are given by (see [31, pp. 142-143])

$$\underline{R}_{L0}^+ = \underline{R}_0^+ + \underline{T}_0^- \cdot \underline{K}_{12} \; , \tag{26}$$

$$\underline{R}_{L0}^- = \underline{R}_L^- + \underline{T}_L^+ \cdot \underline{K}_{21} \; , \tag{27}$$

$$\underline{T}_{L0}^+ = \underline{T}_L^+ \cdot \underline{K}_{22} \; , \tag{28}$$

$$\underline{T}_{L0}^- = \underline{T}_0^- \cdot \underline{K}_{11} \; , \tag{29}$$

and

$$\begin{pmatrix} \underline{K}_{11} & \underline{K}_{12} \\ \underline{K}_{21} & \underline{K}_{22} \end{pmatrix} = \begin{pmatrix} \underline{1} & -\underline{R}_L^+ \\ -\underline{R}_0^- & \underline{1} \end{pmatrix}^{-1} \cdot \begin{pmatrix} \underline{T}_L^- & \underline{0} \\ \underline{0} & \underline{T}_0^+ \end{pmatrix} . \tag{30}$$

The procedure of combining $\underline{S}_L$ and $\underline{S}_0$ to form $\underline{S}_{L0}$ using (25)–(30) uniquely defines a binary associative operation $\circ$, as any two matrices of equal size can be combined in this way. Specifically, we define $\underline{S}_L \circ \underline{S}_0 = \underline{S}_{L0}$. It follows, that the scattering matrix of the entire mass loading floe $\underline{S}$ is

$$\underline{S} = \underline{S}_L \circ \underline{S}_0 \circ \underline{S}_R \, . \tag{31}$$

3.4. Transmission and reflection coefficients

We are primarily interested in the transmission and reflection coefficients of the floe. They are given by the amplitudes of the transmitted and reflected propagating wave modes, normalised by the ingoing wave amplitude (see (9) and (10)), i.e.

$$T = |S_{0,0}| \quad \text{and} \quad R = |S_{N_\zeta+1,0}| \, , \tag{32}$$

respectively, where $S_{i,j}$ denotes the entry of the matrix $\underline{S}$ in the $(1+i)^{\text{th}}$ row and $(1+j)^{\text{th}}$ column.

4. Random length scattering

We now randomize the floe length L by writing

$$L = L_0 + L_1\,\alpha\ , \tag{33}$$

where $0 < L_1 < L_0$, and α is a random variable drawn from some given probability distribution $\mathcal{D}$ constrained to the interval $[-1, 1]$. The deterministic boundary value problem described in §3 then becomes a stochastic boundary value problem. In particular, the reflection coefficient R and the transmission coefficient T now depend on the random variable α. Our objective is to compute the expectation values and variances of $R(\alpha)$ and $T(\alpha)$.

To accomplish this goal we employ the framework of generalised polynomial chaos (gPC), which is expected to converge significantly faster than the traditional Monte Carlo (MC) approach [19]. In the MC method the deterministic problem described in §3 is solved for a large number of randomly selected floe lengths and mean and variance are obtained from that solution sample. The error of this method is known to converge with the inverse square root of the sample size. In contrast, when the dependence of the solutions on the random variable(s) is sufficiently smooth, the gPC methods often show exponential convergence behaviour, although there exists no rigorous mathematical proof of this, to our knowledge.

The key to the gPC technique is the expansion of the α-dependent quantities in terms of a particular polynomial basis $\{P_n(\alpha), n \in \mathbb{N}\}$, which is optimal (in a sense explained below) for the probability distribution $\mathcal{D}$ of α. The polynomials $P_n(\alpha)$ are constructed, for example using the Gram Schmidt algorithm, to be orthonormal with respect to the scalar product

$$\langle f_1, f_2\rangle_\alpha = \int_{-1}^{+1} f_1(\alpha)\, f_2(\alpha)\, \mathrm{PDF}[\mathcal{D}](\alpha)\, \mathrm{d}\alpha\ , \tag{34}$$

where $\mathrm{PDF}[\mathcal{D}]$ is the probability density function of the distribution $\mathcal{D}$. Specifically,

$$\langle P_i, P_j\rangle_\alpha = \delta_{ij}\ , \tag{35}$$

where δ_{ij} is the Kronecker delta. For many of the common probability distributions, however, the corresponding polynomial basis is well established [19]. We refer to the $\{P_n(\alpha)\}$ as gPC polynomials.

The polynomial basis $\{P_n(\alpha)\}$ is optimal in the following sense. Let the reflection coefficient $R(\alpha)$ be expanded in this basis, that is

$$R(\alpha) \approx \sum_{n=0}^{N_P} R_n \, P_n(\alpha) \ , \tag{36}$$

where we only take a finite number of $N_P + 1$ polynomials into account. Then it can be shown that the truncated expression on the right hand side of (36) not only converges to $R(\alpha)$ as $N_P \to \infty$, but it also minimises the L^2 norm error of any same degree polynomial approximation [19, eq. 5.9].

The family of gPC techniques admits two main branches: stochastic collocation (SC) methods, and the stochastic Galerkin (SG) scheme. In the following two subsections we demonstrate both methods by solving the random length problem.

4.1. Stochastic collocation method

We first discuss the stochastic collocation (SC) method [19, 32]. This method is non-intrusive, i.e. it utilizes the deterministic solver described in §3 and is therefore straightforward to implement.

The first step is to solve the fixed length scattering problem described in §3 for $N_C + 1$ different floe lengths $L = L_0 + L_1 \, \alpha_m$, with $m = 0, .., N_C$.

Setting $N_C = N_P$, using the orthonormality condition (35) and the expansion (36) of the reflection coefficient, we find

$$R_m = \int_{-1}^{1} d\alpha \ \mathrm{PDF}[\mathcal{D}](\alpha) \ P_m(\alpha) \, R(\alpha) \approx \sum_{i=0}^{N_P} w_i \ P_m(\alpha_i) \, R(\alpha_i) \ , \tag{37}$$

where the α_i are the roots of $P_{N_P+1}(\alpha)$, and w_i are the quadrature weights for $\mathrm{PDF}[\mathcal{D}]$. An efficient way of computing the α_i and w_i is described in [33]. Alternatively, the expansion (36) could be used to obtain a linear system of $N_C + 1$ equations in $N_P + 1$ variables, which could then be solved directly or

with a least squares method if $N_P < N_C$. Both methods perform equally well as the bulk of the computation time is spent on the evaluations of $R(\alpha_i)$. Here we choose the quadrature method for its superior robustness and the convenience that we have to discuss convergence in only one numerical parameter N_P.

The orthonormality relation (35) can then be used to find the expectation $\mathbb{E}(R) = R_0$ and variance $\mathbb{V}\mathrm{ar}(R) = \sum_{n=1}^{N_P} R_n^2$ of the reflection coefficient. The function $R(\alpha) = |S_{N_{\zeta+1},0}(\alpha)|$ may not be differentiable at all α, however, due to the absolute value in (32), in which case the polynomial approximation converges poorly. To remedy this possible issue we instead expand the underlying complex amplitude $a(\alpha) = S_{N_{\zeta+1},0}(\alpha)$ into gPC polynomials, i.e.

$$a(\alpha) = \sum_{n=0}^{N_P} a_n \, P_n(\alpha) \ . \tag{38}$$

We can then compute the expectation value of $R = |a|$ as

$$\mathbb{E}(R) = \mathbb{E}(|a|) = \int_{-1}^{+1} |a(\alpha)| \, \mathrm{PDF}[\mathcal{D}](\alpha) \, d\alpha \ , \tag{39}$$

which can be estimated using numerical integration. Alternatively, one could compute the expectation value and variance of $\log R^2$ and $\log T^2$. Bennetts and Squire [31] show that the log-averaged transmission coefficient $\mathbb{E}(\log T^2)$ of a single floe gives information about the scattering of an infinite series of floes whose lengths are uniformly randomly distributed. In §5.4 we show, however, that these results are not valid for other length distributions and since we are concerned with only a single floe we consider the quantities $\mathbb{E}(R)$, $\mathbb{V}\mathrm{ar}(R)$, etc., which are easier to interpret. We also remark that semi-analytic expressions for $\mathbb{E}(T)$ and $\mathbb{E}(R)$ can be derived if L_1 is an integer multiple of the ice covered propagating wavelength and L is sufficiently large so that the effect of evanescent modes can be neglected (see [34] and references therein). We made sure that the $\mathbb{E}(T)$ computed with the semi-analytic expression given in [34] agrees with our gPC results when these conditions are satisfied.

Note, that orthonormality of the gPC polynomials cannot be used to simplify

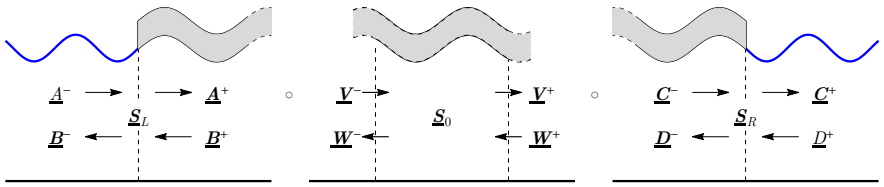

Figure 3: Separation of the stochastic scattering problem into three sub-problems.

the integral in (39). It can be used to simplify the second moment, however, i.e.

$$\begin{aligned}\mathbb{V}\mathrm{ar}(R) &= \int_{-1}^{+1} |a(\alpha)|^2 \,\mathrm{PDF}[\mathcal{D}](\alpha)\; d\alpha - \mathbb{E}(R)^2 \\ &\approx \sum_{m,n=0}^{N_P} a_m\, a_n^* \int_{-1}^{+1} P_m(\alpha)\, P_n(\alpha)\,\mathrm{PDF}[\mathcal{D}](\alpha)\; d\alpha - \mathbb{E}(R)^2 \\ &= \sum_{n=0}^{N_P} |a_m|^2 - \mathbb{E}(R)^2\;, \end{aligned} \tag{40}$$

where a_n^* is the complex conjugate of a_n. The results for the transmission coefficient $T(\alpha)$ follow analogously.

In §5.1 we implement the SC method by expanding the complex amplitudes underlying the reflection and transmission coefficients into gPC modes.

4.2. Stochastic Galerkin method

In this section we introduce the stochastic Galerkin (SG) method to solve the problem of water wave scattering by a floe of random length. In contrast to the SC method described in §4.1, the SG method does not build upon the deterministic solver outlined in §3. Instead, the solution method used to solve the fixed length problem is amended to account for the dependence of the complex wave amplitudes on the random variable α.

Similarly to the fixed length case, we decompose the scattering problem into three sub-problems, illustrated in figure 3, i.e. (i) scattering from the left edge, (ii) propagation of the plane wave solutions in the random domain under the floe, and (iii) scattering from the right edge. As in the fixed length case, each process can be described by a scattering matrix.

4.2.1. Scattering from the floe's edges

The solution method of the left edge scattering problem is similar to that described in §3.1 for the fixed length floe. The potential expansions (11) and (12) only need to be amended to account for their dependence on the random variable α. In the free surface region, only the left-travelling wave amplitudes $\underline{B}^-$ depend on α as the right-travelling modes are incident from $-\infty$ and therefore do not depend on the geometry of the floe. In the ice-covered region, both $\underline{A}^+$ and $\underline{B}^+$ depend on α. Using the gPC framework, we expand these amplitudes in the gPC polynomial basis $\{P_i(\alpha)\}$. Specifically,

$$\begin{aligned}\underline{A}^+(\alpha) &= \big(A_0^+(\alpha), \dots, A_{N_\zeta}^+(\alpha)\big)^{\mathrm{T}} \\ &= \Big(\sum_{i=0}^{N_P} A_{0,i}^+ P_i(\alpha), \dots, \sum_{i=0}^{N_P} A_{N_\zeta,i}^+ P_i(\alpha)\Big)^{\mathrm{T}} \\ &= \big(\boldsymbol{A}_0^+ \cdot \boldsymbol{P}(\alpha), \dots, \boldsymbol{A}_{N_\zeta}^+ \cdot \boldsymbol{P}(\alpha)\big)^{\mathrm{T}} \,, \end{aligned} \tag{41}$$

where $\boldsymbol{A}_n^+$, $n = 0, \dots, N_\zeta$, are row vectors of length $N_P + 1$ containing the amplitudes $A_{n,i}^+$ and $\boldsymbol{P}(\alpha)$ is the column vector of $N_P + 1$ gPC poynomials. Similarly, we have

$$\underline{B}^\pm = \big(\boldsymbol{B}_0^+ \cdot \boldsymbol{P}(\alpha), \dots, \boldsymbol{B}_{N_\zeta}^+ \cdot \boldsymbol{P}(\alpha)\big)^{\mathrm{T}} \,, \tag{42}$$

where $\boldsymbol{B}_n^\pm$, $n = 0, \dots, N_\zeta$, are the row vectors of amplitudes $B_{n,i}^\pm$. Note that we use bold symbols to represent vectors and matrices in the gPC space, as opposed to the underlined symbols defined in §3, which represent vectors and matrices in the vertical mode space. Using this matrix notation, the general solutions (11) and (12) to Laplace's equation on the left and right side of the edge, respectively, become

$$\begin{aligned}\phi(x, z; \alpha) &\approx \phi^-(x, z; \alpha) \\ &= \sum_{n=0}^{N_\zeta} \big(A_n^- \, e^{\mathrm{i}\,\kappa_n\, x} + \boldsymbol{B}_n^- \cdot \boldsymbol{P}(\alpha)\, e^{-\mathrm{i}\,\kappa_n\, x}\big)\, \varsigma_n(z) \,, \qquad x \le 0 \,, \end{aligned} \tag{43}$$

on the left (open water) side and

$$\phi(x,z;\alpha) \approx \phi^+(x,z;\alpha)$$
$$= \sum_{n=0}^{N_\zeta} \left(\boldsymbol{A}_n^+ \, e^{\mathrm{i}\, k_n \, x} + \boldsymbol{B}_n^+ \, e^{-\mathrm{i}\, k_n \, x}\right) \cdot \boldsymbol{P}(\alpha)\, \zeta_n(z) \;, \qquad x \geq 0 \;, \tag{44}$$

on the right (ice-covered) side.

The matching of the potential and normal velocity at $x = 0$ can be done for each gPC mode independently. The scattering matrix of the left edge can therefore be expressed directly in terms of the reflection and transmission block components of the scattering matrix $\underline{S}_L$ given in (17) and (18) for the fixed length problem. Specifically, we can write the mapping of wave mode amplitudes on either side of the edge as

$$\underline{\boldsymbol{A}}^+ = \underline{\boldsymbol{T}}_L^- \cdot \underline{A}^- + \underline{\boldsymbol{R}}_L^+ \cdot \underline{\boldsymbol{B}}^+ \;, \tag{45}$$

$$\underline{\boldsymbol{B}}^- = \underline{\boldsymbol{R}}_L^- \cdot \underline{A}^- + \underline{\boldsymbol{T}}_L^+ \cdot \underline{\boldsymbol{B}}^+ \;. \tag{46}$$

where the vectors $\underline{\boldsymbol{A}}^+ = (\boldsymbol{A}_0^+, \ldots, \boldsymbol{A}_{N_\zeta}^+)^{\mathrm{T}}$ and $\underline{\boldsymbol{B}}^\pm = (\boldsymbol{B}_0^\pm, \ldots, \boldsymbol{B}_{N_\zeta}^\pm)^{\mathrm{T}}$ have length $(N_\zeta + 1)(N_P + 1)$.

The blocks $\underline{T}_L^\pm$ and $\underline{R}_L^\pm$ of $\underline{S}_L$ must also be amended to operate on the product space of vertical and gPC modes, while leaving the gPC modes unaffected. Therefore the matrices $\underline{\boldsymbol{T}}_L^+$ and $\underline{\boldsymbol{R}}_L^+$ are given by

$$\underline{\boldsymbol{R}}_L^+ = \underline{R}_L^+ \otimes \mathbf{1} \qquad \text{and} \qquad \underline{\boldsymbol{T}}_L^+ = \underline{T}_L^+ \otimes \mathbf{1} \;, \tag{47}$$

where $\mathbf{1}$ is the identity matrix of dimension $(N_P + 1) \times (N_P + 1)$. The operation $\otimes$ is the Kronecker product, which is the matrix representation of the tensor product. Effectively, every entry $(\underline{R}_L^+)_{ij}$ is replaced by the diagonal block $(\underline{R}_L^+)_{ij}\, \mathbf{1}$ and the same is done for $\underline{T}_L^+$. Since $\underline{A}^-$ does not depend on α, it can only influence the zeroth order term $P_0(\alpha) = 1$ in the gPC expansions of $\underline{A}^+$ and $\underline{B}^-$. Therefore, the matrices $\underline{R}_L^-$ and $\underline{T}_L^-$ acting on $\underline{A}^-$ are expressed as

$$\underline{\boldsymbol{R}}_L^- = \underline{R}_L^- \otimes \boldsymbol{e}_0 \qquad \text{and} \qquad \underline{\boldsymbol{T}}_L^- = \underline{T}_L^- \otimes \boldsymbol{e}_0 \;, \tag{48}$$

where $\boldsymbol{e}_0$ is the unit column vector in the space of gPC polynomials which corresponds to $P_0(\alpha) = 1$, with size $(N_P + 1)$. Effectively, every entry $(\underline{R}_L^-)_{ij}$

is replaced with the column vector $((\underline{R}_L^-)_{ij}, 0, \ldots, 0)^{\mathrm{T}}$ and the same is done for $\underline{T}_L^-$. The scattering matrix $\underline{\boldsymbol{S}}_L$ of the left edge can be assembled from these four blocks, i.e.

$$\begin{pmatrix} \underline{\boldsymbol{A}}^+ \\ \underline{\boldsymbol{B}}^- \end{pmatrix} = \underline{\boldsymbol{S}}_L \cdot \begin{pmatrix} \underline{A}^- \\ \underline{\boldsymbol{B}}^+ \end{pmatrix} = \begin{pmatrix} \underline{\boldsymbol{T}}_L^- & \underline{\boldsymbol{R}}_L^+ \\ \underline{\boldsymbol{R}}_L^- & \underline{\boldsymbol{T}}_L^+ \end{pmatrix} \cdot \begin{pmatrix} \underline{A}^- \\ \underline{\boldsymbol{B}}^+ \end{pmatrix} \ . \tag{49}$$

It relates the gPC modes of the wave amplitudes A_n^- and $B_n^+(\alpha)$ to the gPC modes of the wave amplitudes $A_n^+(\alpha)$ and $B_n^-(\alpha)$.

As in the fixed length case, the symmetry of the problem allows us to construct the right-edge scattering matrix $\underline{\boldsymbol{S}}_R$ from the block components of $\underline{\boldsymbol{S}}_L$.

4.2.2. Wave propagation in a random domain

In §3.2 we constructed the matrix $\underline{S}_0$, which describes the phase change of the wave modes between the two edges $x = 0$ and $x = L$. We now seek a mapping $\underline{\boldsymbol{S}}_0$ describing the phase change of the wave modes when the boundary $x = L(\alpha)$ is only given in terms of the probability distribution of α.

To that end, we follow Xiu and Tartakovsky [35] by first transforming the deterministic governing equations with a random boundary into stochastic equations with a fixed boundary. This is accomplished by expressing the Laplace equation (1) in a new α-dependent coordinate system $(\tilde{x}, z)$, defined by

$$\tilde{x}(x;\alpha) = s(\alpha)\, x \qquad \text{with} \qquad s(\alpha) = \frac{L_0}{L_0 + L_1\, \alpha} \ , \tag{50}$$

which is chosen such that the left and right floe edges always have the coordinates $\tilde{x} = 0$ and $\tilde{x} = L_0$, respectively. In this new coordinate system, Laplace's equation (1) becomes

$$-s^2(\alpha)\, \partial_{\tilde{x}}^2 \phi = \partial_z^2 \phi \ , \tag{51}$$

while the ice-covered surface and sea floor boundary conditions (6) and (7) remain unchanged. In the horizontal direction, the solution must be matched

in ϕ and $\partial_x \phi$ to

$$\begin{aligned}\phi(x,z;\alpha) &\approx \phi^L(x,z;\alpha) \\ &= \sum_{n=0}^{N_\zeta} \left(\boldsymbol{V}_n^- \, e^{\mathrm{i}\, k_n \, x} + \boldsymbol{W}_n^- \, e^{-\mathrm{i}\, k_n \, x} \right) \cdot \boldsymbol{P}(\alpha) \, \zeta_n(z) \; , \qquad x = 0 \; , \end{aligned} \tag{52}$$

at $x = \tilde{x} = 0$, which is analogous to equation (21) in the fixed length problem, and to

$$\begin{aligned}\phi(x,z;\alpha) &\approx \phi^R(x,z;\alpha) \\ &= \sum_{n=0}^{N_\zeta} \left(\boldsymbol{V}_n^+ \, e^{\mathrm{i}\, k_n \, x} + \boldsymbol{W}_n^+ \, e^{-\mathrm{i}\, k_n \, x} \right) \cdot \boldsymbol{P}(\alpha) \, \zeta_n(z) \; , \qquad x = L \; , \end{aligned} \tag{53}$$

at $x = L$ (or equivalently $\tilde{x} = L_0$), analogous to (22). We introduced the row vectors $\boldsymbol{V}_n^\pm$ and $\boldsymbol{W}_n^\pm$ of length $N_P + 1$ containing the gPC coefficients of $V_n^\pm(\alpha)$ and $W_n^\pm(\alpha)$ for each vertical mode $n = 0, \ldots, N_\zeta$.

To find the general solution of the stochastic Laplace equation (51), we separate variables by invoking the ansatz

$$\phi(\tilde{x}, z; \alpha) = \zeta(z) \, \varphi(\tilde{x}; \alpha) \; . \tag{54}$$

The vertical solutions ζ_n are the same as for the deterministic problem, given by equation (14). In the horizontal direction we obtain

$$s^2(\alpha) \, \partial_{\tilde{x}}^2 \varphi(\tilde{x}; \alpha) = -k^2 \, \varphi(\tilde{x}, \alpha) \; . \tag{55}$$

We expand φ in the gPC polynomial basis

$$\varphi(\tilde{x}; \alpha) \approx \sum_{j=0}^{N_P} \xi_j(\tilde{x}) \, P_j(\alpha) \; , \tag{56}$$

where the infinite series has been truncated to contain $N_P + 1$ terms. Substituting (56) into equation (55), dividing by $s^2(\alpha)$, and projecting on P_i using the gPC scalar product (34), results in

$$\partial_{\tilde{x}}^2 \xi_i(\tilde{x}) = -k^2 \sum_{j=0}^{N_P} \xi_j(\tilde{x}) \, \langle P_i, s^{-2} \, P_j \rangle_\alpha \; , \tag{57}$$

where we have used the orthonormality (35) of the gPC polynomials. We define the row vector $\boldsymbol{\xi}$ of length N_P+1 and the square matrix $\boldsymbol{M}$ of size $(N_P+1)\times(N_P+1)$, with entries given by $\boldsymbol{\xi}\cdot\boldsymbol{e}_i=\xi_i(\tilde{x})$, and $\boldsymbol{e}_i^{\mathrm{T}}\cdot\boldsymbol{M}\cdot\boldsymbol{e}_j=\langle P_i,s^{-2}\,P_j\rangle_\alpha$, respectively, where $\boldsymbol{e}_i$ corresponds to the i^{th} unit vector in the gPC standard basis. This allows us to rewrite (57) in matrix form as

$$\partial_{\tilde{x}}^2\,\boldsymbol{\xi}=-k^2\,\boldsymbol{\xi}\cdot\boldsymbol{M}\ . \tag{58}$$

The matrix $\boldsymbol{M}$ is real and symmetric, so there exists a unitary matrix $\boldsymbol{U}$ such that $\boldsymbol{M}=\boldsymbol{U}\cdot\not{\boldsymbol{M}}\cdot\boldsymbol{U}^{-1}$, where $\not{\boldsymbol{M}}$ is diagonal. Thus, we can write

$$\partial_{\tilde{x}}^2\,\boldsymbol{\xi}=-k^2\,\boldsymbol{\xi}\cdot\boldsymbol{U}\cdot\not{\boldsymbol{M}}\cdot\boldsymbol{U}^{-1}\ , \tag{59}$$

$$\partial_{\tilde{x}}^2\,\boldsymbol{\xi}\cdot\boldsymbol{U}=-k^2\,\boldsymbol{\xi}\cdot\boldsymbol{U}\cdot\not{\boldsymbol{M}}\ , \tag{60}$$

$$\partial_{\tilde{x}}^2\,\boldsymbol{X}=-k^2\,\boldsymbol{X}\cdot\not{\boldsymbol{M}}\ , \tag{61}$$

where we define the row vector $\boldsymbol{X}=\boldsymbol{\xi}\cdot\boldsymbol{U}$ of length N_P+1. Since $\not{\boldsymbol{M}}$ is diagonal, this is a system of independent ordinary differential equations with general solution

$$\boldsymbol{\xi}=\left(\boldsymbol{V}^0\cdot\exp\left(\mathrm{i}\,k\,\sqrt{\not{\boldsymbol{M}}}\,\tilde{x}\right)+\boldsymbol{W}^0\cdot\exp\left(-\mathrm{i}\,k\,\sqrt{\not{\boldsymbol{M}}}\,\tilde{x}\right)\right)\cdot\boldsymbol{U}^{-1}\ , \tag{62}$$

where $\boldsymbol{V}^0$ and $\boldsymbol{W}^0$ are now vectors of length N_P+1 and where we have used the definition of $\boldsymbol{X}$. The general solution to (51) can therefore be approximated by

$$\begin{aligned}\phi(\tilde{x},z;\alpha)\approx\phi^0(\tilde{x},z;\alpha)&=\sum_{n=0}^{N_\zeta}\zeta_n(z)\,\boldsymbol{\xi}_n(\tilde{x})\cdot\boldsymbol{P}(\alpha)\\&=\sum_{n=0}^{N_\zeta}\zeta_n(z)\left(\boldsymbol{V}_n^0\cdot\exp\left(\mathrm{i}\,k_n\,\boldsymbol{G}\,\tilde{x}\right)+\boldsymbol{W}_n^0\cdot\exp\left(-\mathrm{i}\,k_n\,\boldsymbol{G}\,\tilde{x}\right)\right)\cdot\boldsymbol{U}^{-1}\cdot\boldsymbol{P}(\alpha)\ ,\end{aligned} \tag{63}$$

where we have introduced $\boldsymbol{G}=\sqrt{\not{\boldsymbol{M}}}$.

We are now in a position to construct the random phase change matrix $\underline{\boldsymbol{S}}_0$ by matching the general solution (63) under the floe to the solutions (52) and (53) at $x=0$ and $x=L$. Applying the four matching conditions

$$\phi^L(x,z;\alpha)|_{x=0}=\phi^0(\tilde{x},z;\alpha)|_{\tilde{x}=0}\ , \tag{64}$$

$$\phi^0(\tilde{x},z;\alpha)|_{\tilde{x}=L_0}=\phi^R(x,z;\alpha)|_{x=L}\ , \tag{65}$$

and

$$\partial_x \phi^L(x,z;\alpha)|_{x=0} = s(\alpha)\,\partial_{\tilde{x}}\phi^0(\tilde{x},z;\alpha)|_{\tilde{x}=0}\ , \tag{66}$$

$$s(\alpha)\,\partial_{\tilde{x}}\phi^0(\tilde{x},z;\alpha)|_{\tilde{x}=L_0} = \partial_x \phi^R(x,z;\alpha)|_{x=L}\ , \tag{67}$$

and projecting onto the vertical and gPC modes, we obtain the four matrix equations

$$(\boldsymbol{V}_n^- + \boldsymbol{W}_n^-) = (\boldsymbol{V}_n^0 + \boldsymbol{W}_n^0)\cdot\boldsymbol{U}^{-1}\ , \tag{68}$$

$$(\boldsymbol{V}_n^+ + \boldsymbol{W}_n^+) = (\boldsymbol{V}_n^0\,\exp(\mathrm{i}\,k_n\,\boldsymbol{G}\,L_0) + \boldsymbol{W}_n^0\,\exp(-\mathrm{i}\,k_n\,\boldsymbol{G}\,L_0))\cdot\boldsymbol{U}^{-1}\ , \tag{69}$$

$$(\boldsymbol{V}_n^- - \boldsymbol{W}_n^-)\cdot\boldsymbol{N} = (\boldsymbol{V}_n^0 - \boldsymbol{W}_n^0)\cdot\boldsymbol{G}\cdot\boldsymbol{U}^{-1}\ , \tag{70}$$

$$(\boldsymbol{V}_n^+ - \boldsymbol{W}_n^+)\cdot\boldsymbol{N} = (\boldsymbol{V}_n^0\,\exp(\mathrm{i}\,k_n\,\boldsymbol{G}\,L_0) - \boldsymbol{W}_n^0\,\exp(-\mathrm{i}\,k_n\,\boldsymbol{G}\,L_0))\cdot\boldsymbol{G}\cdot\boldsymbol{U}^{-1}\ . \tag{71}$$

where we have defined the $(N_P+1)\times(N_P+1)$ matrix $\boldsymbol{N}$ with components $\boldsymbol{e}_i^{\mathrm{T}}\cdot\boldsymbol{N}\cdot\boldsymbol{e}_j = \langle P_i, s^{-1}\,P_j\rangle_\alpha$. Eliminating $\boldsymbol{V}_n^0$ and $\boldsymbol{W}_n^0$ from equations (68)–(71), we obtain the mapping

$$\begin{pmatrix}\underline{\boldsymbol{V}}^+\\ \underline{\boldsymbol{W}}^-\end{pmatrix} = \underline{\boldsymbol{S}}_0\cdot\begin{pmatrix}\underline{\boldsymbol{V}}^-\\ \underline{\boldsymbol{W}}^+\end{pmatrix}\ , \tag{72}$$

where the random phase change matrix $\underline{\boldsymbol{S}}_0$ is defined by

$$\underline{\boldsymbol{S}}_0 = \begin{pmatrix} \boldsymbol{T}_0^- & & & \boldsymbol{R}_0^+ & & \\ & \ddots & & & \ddots & \\ & & \boldsymbol{T}_{N_\zeta}^- & & & \boldsymbol{R}_{N_\zeta}^+ \\ \boldsymbol{R}_0^- & & & \boldsymbol{T}_0^+ & & \\ & \ddots & & & \ddots & \\ & & \boldsymbol{R}_{N_\zeta}^- & & & \boldsymbol{T}_{N_\zeta}^+ \end{pmatrix}\ . \tag{73}$$

The blocks $\boldsymbol{T}_n^\pm$ and $\boldsymbol{R}_n^\pm$ are given by

$$\boldsymbol{R}_n^\pm = \boldsymbol{C}_n\cdot(\boldsymbol{E}_n^{-1}\cdot\boldsymbol{F}^- - \boldsymbol{F}^-\cdot(\boldsymbol{F}^+)^{-1}\cdot\boldsymbol{E}_n\cdot\boldsymbol{F}^+)\ , \tag{74}$$

$$\boldsymbol{T}_n^\pm = \boldsymbol{C}_n\cdot(\boldsymbol{F}^+ - \boldsymbol{F}^-\cdot(\boldsymbol{F}^+)^{-1}\cdot\boldsymbol{F}^-)\ , \tag{75}$$

where

$$\boldsymbol{F}^{\pm} = \boldsymbol{U}^{-1} \pm \boldsymbol{G} \cdot \boldsymbol{U}^{-1} \cdot \boldsymbol{N}^{-1} \,, \tag{76}$$

$$\boldsymbol{C}_n = \left(\boldsymbol{E}_n^{-1} \, \boldsymbol{F}^{+} - \boldsymbol{F}^{-} \cdot (\boldsymbol{F}^{+})^{-1} \cdot \boldsymbol{E}_n \cdot \boldsymbol{F}^{-} \right)^{-1} \,, \tag{77}$$

$$\boldsymbol{E}_n = \exp\left(\mathrm{i}\, k_n \, \boldsymbol{G} \, L_0\right) \,. \tag{78}$$

The matrix $\underline{\boldsymbol{S}}_0$ maps the gPC modes of the amplitudes of the wave modes travelling into the covered region to the gPC modes of the amplitudes of the wave modes travelling out of the covered region, where the effect of the floe edge has not yet been considered. It therefore describes the random phase change of the waves under the floe.

4.2.3. The Random Scattering Matrix

The procedure described in §3.3 to combine scattering matrices remains unchanged in the random length case. Using the operation $\circ$ defined in §3.3 we express the scattering matrix of the random length ice floe as

$$\underline{\boldsymbol{S}} = \underline{\boldsymbol{S}}_L \circ \underline{\boldsymbol{S}}_0 \circ \underline{\boldsymbol{S}}_R \,, \tag{79}$$

which has dimension $2\,(N_\zeta+1)(N_P+1) \times 2\,(N_\zeta+1)$. It relates the α-independent amplitudes of the ingoing waves to the α-dependent amplitudes of the outgoing waves (see figure 3), i.e.

$$\begin{pmatrix} \underline{\boldsymbol{C}}^{+} \\ \underline{\boldsymbol{B}}^{-} \end{pmatrix} = \underline{\boldsymbol{S}} \cdot \begin{pmatrix} \underline{A}^{-} \\ \underline{D}^{+} \end{pmatrix} \,. \tag{80}$$

We use (39) and (40) to calculate the expectation and variance, respectively, of the absolute value of any complex quantity obtained from the SG method. In particular, applying these formulae for the travelling vertical mode amplitudes $C_0^+(\alpha) = \boldsymbol{C}_0^+ \cdot \boldsymbol{P}$ and $B_0^-(\alpha) = \boldsymbol{B}_0^- \cdot \boldsymbol{P}$ gives the statistical central moments of the transmission and reflection coefficients, respectively.

5. Results

We devise a number of numerical tests to establish the performance of the two SC methods described in §4.1 and the SG method described in §4.2, in comparison to the Monte Carlo (MC) approach. The parameters $L_0 = 30\,\mathrm{m}$, $L_1 = 10\,\mathrm{m}$, $H = 100\,\mathrm{m}$, $h = 2\,\mathrm{m}$, and $\omega = 2\,\pi/5\,\mathrm{Hz}$ are fixed for all of the following simulations. This implies, that the travelling wave modes in the open water and floe covered domains have wavelength $\lambda_0 = 2\,\pi/\kappa_0 = 39\,\mathrm{m}$, and $\lambda_0^{\mathrm{ice}} = 2\,\pi/k_0 = 28\,\mathrm{m}$, respectively. We also set the number of evanescent vertical modes to $N_\zeta = 5$ and compute the solution of the matching problem at the floe edges with a sufficient level of certainty to ensure that the transmission coefficient T has converged to six digits of accuracy.

Throughout this article we consider two possible choices for the distribution $\mathcal{D}$ of α: (i) the uniform distribution $\mathcal{U}$ on the interval [-1,1], which we adopt because of its simplicity, and (ii) a beta distribution that has been transformed to be non-zero on the interval [-1,1]. We chose the latter distribution because its probability density function resembles that of a normal distribution while it converges continuously to zero as $\alpha \to \pm 1$. Other probability distributions on $[-1, 1]$ could be used instead. The PDFs of $\mathcal{U}$ and $\mathcal{B}$ are given by

$$\mathrm{PDF}[\mathcal{U}](\alpha) = \frac{1}{2}\,, \tag{81}$$

and

$$\mathrm{PDF}[\mathcal{B}](\alpha) = \frac{2^{1-2m}\left(1-\alpha^2\right)^{m-1}}{B(m,m)}\bigg|_{m=10} = \frac{230945}{131072}\left(1-\alpha^2\right)^9\,, \tag{82}$$

respectively, where $B(m, m)$ is the beta function. Their graphs are shown in the top panel of figures 4 and 5, respectively.

The gPC polynomials corresponding to $\mathcal{U}$ and $\mathcal{B}$, as defined by (34) and (35), are

$$P_n(\alpha) = \sqrt{2n+1}\,\mathcal{P}_n^{(0,0)}(\alpha)\,, \tag{83}$$

and

$$P_n(\alpha) = \frac{\sqrt{(2\,n+19)\,n!\,(n+18)!}}{2\,\sqrt{230945}\,(n+9)!}\,\mathcal{P}_n^{(9,9)}(\alpha)\,, \tag{84}$$

respectively, for $n = 0, \ldots, N_P$, and where $\mathcal{P}_n^{(i,j)}(\alpha)$ are the Jacobi polynomials of degree n [19]. It should be noted that for $i = j = 0$ the Jacobi polynomials $\mathcal{P}_n^{(i,j)}(\alpha)$ reduce to the Legendre polynomials for all non-negative integers n.

First, we illustrate how the probability distribution $R(\mathcal{D})$ of the output reflection coefficient R is related to the probability distribution $\mathcal{D}$ of the input α. Figures 4 and 5 show the reflection coefficient as a function of the parameter α (central panel), which does not depend on the choice of the distribution $\mathcal{D}$. Thus, we constructed the graph by computing several solutions $R(\alpha)$ for different α, using the procedure described in §3. The SC and SG methods provide analytic expressions approximating the function $R(\alpha)$. Via (39) and (40) they also provide the expectation $\mathbb{E}(R)$ and (taking the square root) the standard deviation $\mathbb{V}\mathrm{ar}(R)^{1/2}$, which are displayed as error bars on the right panels of the two figures.

The right panels of figures 4 and 5 also show an approximation to $\mathrm{PDF}[R(\mathcal{D})]$. To compute the latter, we subdivided the range of $R(\alpha)$ into 100 intervals $\{[r_n, r_{n+1}], n = 0, \cdots, 99\}$. For each interval we then estimated the probability that $r_n \leq R < r_{n+1}$ by numerically integrating $\mathrm{PDF}[\mathcal{D}](\alpha)$ over the α-intervals for which $R(\alpha)$ satisfies this condition. Consequently, the extrema of $\mathrm{PDF}[\mathcal{D}](\alpha)$ correspond to discontinuities in $\mathrm{PDF}[R(\mathcal{D})](R)$. These discontinuities are only prominent if $\mathrm{PDF}[\mathcal{D}](\alpha)$ is large at the corresponding extremum, however. Consider for example the discontinuity at $R \approx 0.16$ in figure 4, which is generated from the endpoint minimum of $R(\alpha)$ at $\alpha = 1$. This discontinuity is not visible in figure 5, because the PDF of the beta distribution vanishes with $\alpha \to 1$. We also notice, that $\mathrm{PDF}[R(\mathcal{U})](R)$ is skewed towards large R, as most points of the graph of $R(\alpha)$ lie in the upper half of the range of $R(\alpha)$ and all points are equally weighted by the uniform distribution of α. The $\mathrm{PDF}[R(\mathcal{B})](R)$ is more evenly distributed, because the beta distribution gives more weight to small $R(\alpha)$. Consequently, the expectation value of R is lower for $\alpha \sim \mathcal{B}$ than it is for $\alpha \sim \mathcal{U}$.[1]

[1] We use the standard notation in statistics where $\sim$ stands for "has the probability distri-

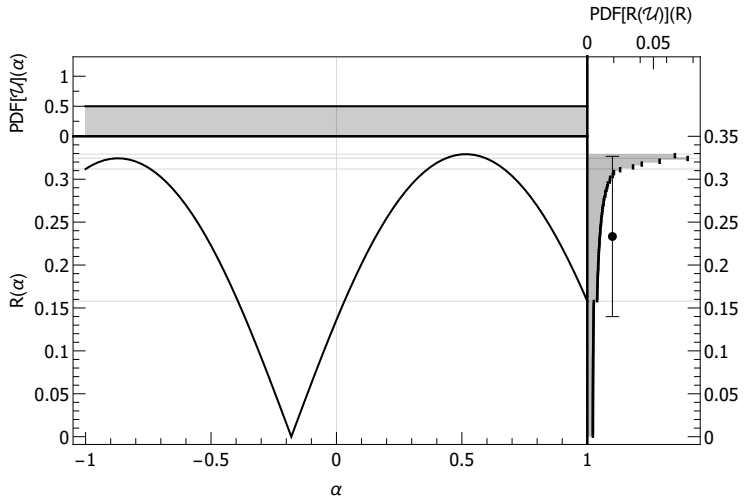

Figure 4: Transformation of the probability distribution. The top panel shows the uniform probability density function for the random length parameter $\alpha \sim \mathcal{U}$. The central panel shows the reflection coefficient R as a function of α. The right panel shows the histogram of the probability distribution of $R(\mathcal{U})$. The point and error bar represent the expected $R \pm$ its standard deviation as computed by the stochastic Galerkin method.

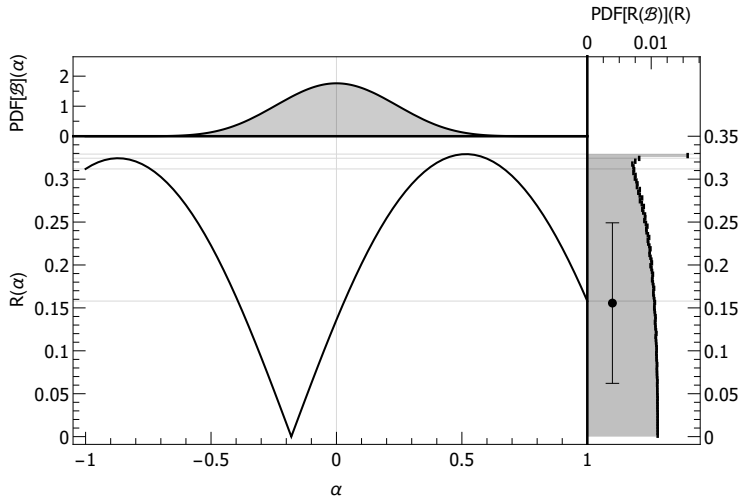

Figure 5: Same as figure 4, but with α following the transformed beta distribution $\mathcal{B}$.

$\mathcal{D}$	method	$\mathbb{E}(T)$	$\mathbb{V}\mathrm{ar}(T)$	$\mathbb{E}(R)$	$\mathbb{V}\mathrm{ar}(R)$	timing in s
$\mathcal{U}$	SC	10	9	17	14	0.90
$\mathcal{U}$	SG	9	9	16	13	0.76
$\mathcal{B}$	SC	7	7	14	10	0.82
$\mathcal{B}$	SG	7	6	13	9	2.2

Table 1: Numerical parameters and computation times of the two gPC methods. The integers give the smallest number of gPC polynomials $N = N_P (= N_C)$ necessary to achieve six digit accuracy in the quantity of the respective column. The timings have been estimated using the maximum N_P in the respective row, such that all quantities are computed with at least six digit accuracy. The Monte Carlo (MC) method did not converge to comparable accuracy (see figures 9 and 10) after 60 s and therefore is not included in the table.

5.1. Stochastic collocation method

We implement the SC method by expanding the complex amplitudes, corresponding to the reflection and transmission coefficients, into N_P gPC modes.

Figure 6 shows the error of the SC method for various numbers of collocation points $N = N_C = N_P$. The case $\alpha \sim \mathcal{U}$ is shown on the left side (panel a), and the case $\alpha \sim \mathcal{B}$ is shown on the right side (panel b). For both distributions of α the computed central moments of the transmission coefficient T and the reflection coefficient R converge exponentially, at least up to some $N = N_{\mathrm{crit}}$. For the expectation and variance of T we find $N_{\mathrm{crit}} = 16$ for both distributions of α. Beyond N_{crit} the error Δ increases exponentially (at a slow rate) when $\alpha \sim \mathcal{U}$ and stays constant at $\Delta \approx 10^{-13}$ when $\alpha \sim \mathcal{B}$. For the expectation and variance of R we find $N_{\mathrm{crit}} \geq 25$ when $\alpha \sim \mathcal{U}$ (not shown) and $N_{\mathrm{crit}} = 20$ when $\alpha \sim \mathcal{B}$. In the latter case the error Δ stays roughly constant at $\Delta \approx 5 \times 10^{-10}$ for $N \geq N_{\mathrm{crit}}$.

5.2. Stochastic Galerkin method

Figure 7 illustrates the convergence of the SG method. When $\alpha \sim \mathcal{U}$ the central moments of $R(\mathcal{U})$ and $T(\mathcal{U})$ converge exponentially in expectation and

bution of".

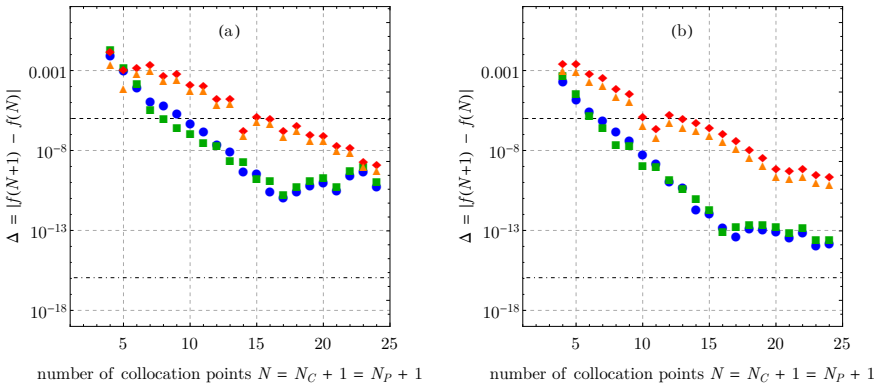

Figure 6: Estimated accuracy of the SC method. Successive differences in transmission expectation (blue circles), transmission variance (green squares), reflection expectation (red diamonds), and reflection variance (orange triangles), as the number of gPC modes and collocation points $N = N_C = N_P$ is increased. The random variable α follows the uniform distribution $\mathcal{U}$ in panel (a), and the transformed beta distribution $\mathcal{B}$ in panel (b). Horizontal dashed and dash-dotted lines indicate the convergence goal 10^{-6} and machine precision $\sim 10^{-16}$, respectively.

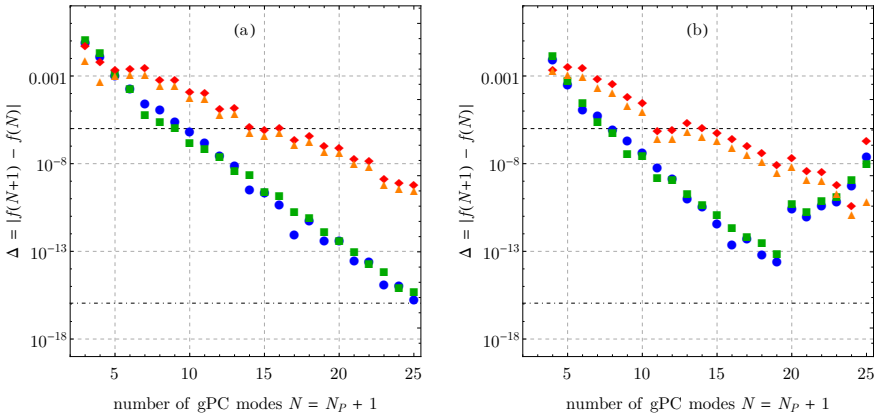

Figure 7: Same as figure 6, but for the SG method.

variance. When $\alpha \sim \mathcal{B}$ the exponential convergence of the central moments of $R(\mathcal{B})$ stops at 10^{-13} with $N = N_{\text{crit}} = 19$. For larger N the large numbers occurring in the expression (84) result in an error increase. For $N > 25$ ill-conditioned matrices lead to a breakdown of the SG algorithm.

We consider the solution converged, if all solutions computed with larger N_P differ from it by less than 10^{-6}. The number of gPC modes $N_P + 1$ necessary for six digits of accuracy is given in table 1 for each quantity of interest.

5.3. Comparison of performances

Both gPC methods show exponential convergence up to some $N = N_{\text{crit}}$, thereby achieving at least nine digits of precision in the central moments of the reflection and transmission coefficients.

Figure 8 shows the exponential convergence rates γ against N_{crit}, assuming the error $\Delta \propto \exp(-\gamma N_P)$ for all $N_P \leq N_{\text{crit}}$. In every case γ lies between 0.6 and 1.8. We always find γ and N_{crit} for the expectation value of a quantity close to the γ and N_{crit} for its variance. This is expected, as expectation and variance are both computed from the same gPC expansions using equations (39) and (40). Computation of R generally converges slower. This is also not surprising, as the value of R is small compared to the value of T, which implies

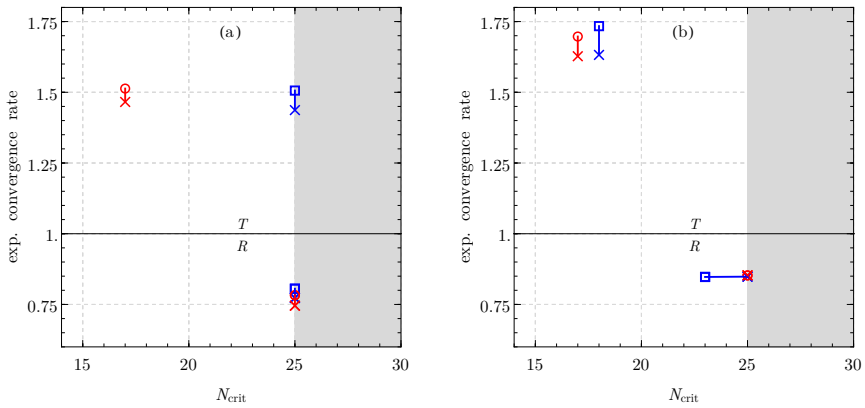

Figure 8: Exponential convergence rates of the gPC methods against N_{crit}, where convergence is exponential for all $N_P \leq N_{\mathrm{crit}}$. The two panels (a) and (b) contain results for $\alpha \sim \mathcal{U}$ and $\alpha \sim \mathcal{B}$, respectively. Expectation values of T (above 1) and R (below 1), computed with the SG (blue rectangles) and SC (red circles) method are connected by a line with the corresponding variances, indicated by a cross. Convergence has not been tested beyond $N_P = 25$.

that high precision is needed to achieve the same accuracy. Overall, the SC and SG methods show similar convergence properties, except when we compute the moments of T with $\alpha \sim \mathcal{U}$, where the SG method converges to much higher precision (larger N_{crit}) than the SC method. This may change, however, with different period, floe thickness, or water depth settings.

We estimated average computation times using a machine with an Intel$^{\mathrm{R}}$ Core$^{\mathrm{TM}}$ i7-3517U CPU (2.4 GHz) and 10 GB RAM (WolframMark$^{\mathrm{TM}}$ benchmark 0.78). The timings for the gPC methods are listed in table 1.

When $\alpha \sim \mathcal{U}$ the SC and SG methods show similar performance, while when $\alpha \sim \mathcal{B}$ the SG method is significantly slower.

One has to keep in mind, however, that the SG method returns much more information than the SC methods. Specifically, it gives an approximation to the functional dependence of all outgoing complex amplitudes on the random parameter α (see equation (80)). Furthermore, formulae (39) and (40) can be used, respectively, to compute the expectation and variance of the outgoing

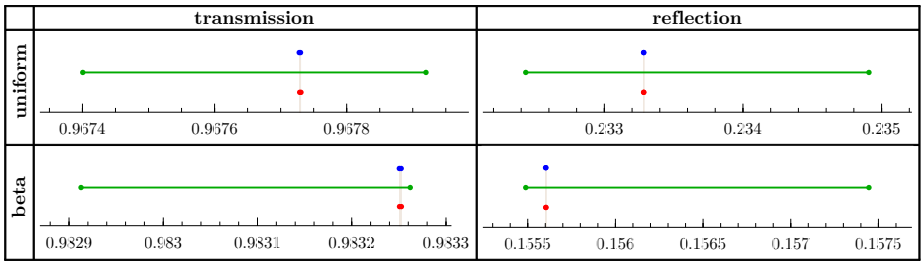

Figure 9: Expectation values, as predicted by the SG (blue), MC (green), and SC (red) methods (top to bottom in each panel). The intervals signify the accuracies with which these results were obtained.

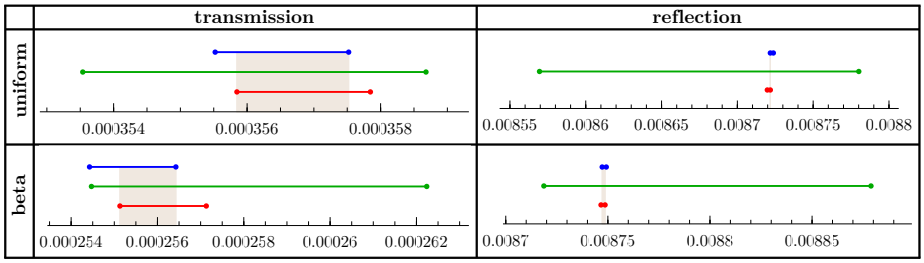

Figure 10: Same as figure 9, but for variances.

evanescent wave mode amplitudes.

Figures 9 and 10 show, for the two probability distributions $\mathcal{U}$ and $\mathcal{B}$, the expectations and variances of R and T, respectively, computed with the three different methods, i.e. SG, SC, and MC. In the MC approach we compute the R and T for 10^4 values of α which are sampled from either $\mathcal{U}$ or $\mathcal{B}$. This takes about 60 s. Expectation and variance are estimated from this sample. The displayed interval is defined as mean $\pm$ standard deviation, estimated from 10 individual MC runs with different random seeds, each of which takes about 60 s.

The results of all three methods are compatible within their respective accuracies. That is, six digits for all gPC methods and significantly larger intervals for the MC method, despite its runtime being more than 20 times greater than the runtime of any of the gPC methods.

5.4. Uniform vs. beta distribution

The good performance of the gPC methods allows us to compute results for a large variety of parameters, such as wave frequency and floe thickness. Each of the two panels of figure 11 shows an overlay of two contour plots in the space of these two parameters. The shaded contours in the background represent the reflection coefficient R, computed for a fixed floe length $L = 38\,\mathrm{m}$.

We note that the minima (dark areas) correspond to regions where the floe length is commensurable with the ice covered water wavelength $\lambda_0^{\mathrm{ice}} < \lambda_0$, where reflection is especially low.

The white dashed lines indicate the contours of the expected reflection coefficient $\mathbb{E}(R)$, assuming either $\alpha \sim \mathcal{U}$ (left panel a), or $\alpha \sim \mathcal{B}$ (right panel b). These contours are computed by running the SC method to calculate $\mathbb{E}(R)$ for more than 1000 parameter pairs, where we ensured that each computation converged to at least three digits of accuracy. We chose $L_0 = 38\,\mathrm{m}$ (as for the fixed length countours in the background) and $L_1 = 20\,\mathrm{m}$ throughout. One can clearly see that the $\mathbb{E}(R)$ contours are very similar to those of R when α follows the transformed beta distribution $\mathcal{B}$, which is peaked around $L = L_0$. In contrast, when α follows a uniform distribution the $\mathbb{E}(R)$ contours are "smeared out".

The discrepancy in $\mathbb{E}(R)$ between the two distributions is an important observation. For instance, when Bennetts and Squire [31] calculate the expected transmission of an array of ice floes of random lengths, they assume the floe lengths to be uniformly distributed, whereas real ice floe sizes are believed to follow a power law distribution [17]. Figure 11 shows that this can make a significant difference. Although our results were computed for the mass loading model, there is no reason to expect this fact to change when e.g. elasticity is included in the floe model.

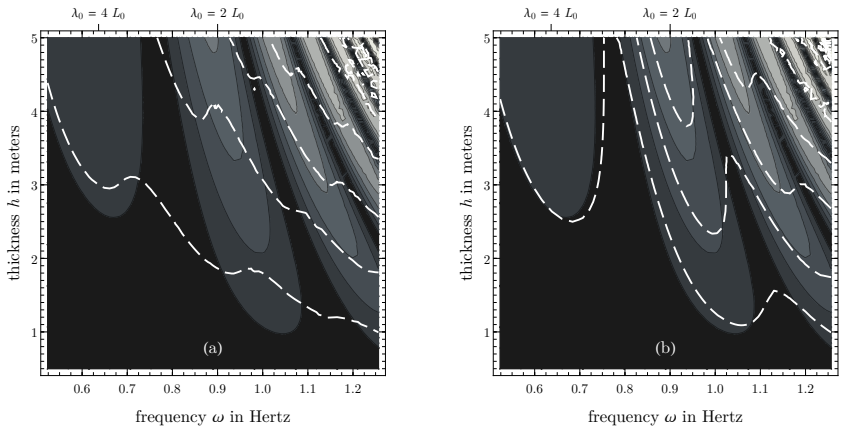

Figure 11: Contours of $R(2\pi/\omega, h)$ (shaded) overlayed with contours of $\mathbb{E}[R](2\pi/\omega, h)$ (white dashed lines) for (a) $\alpha \sim \mathcal{U}$ and (b) $\alpha \sim \mathcal{B}$. The fixed length result R is computed for $L = 38\,\mathrm{m}$. For the expectation values we assume the same mean length, i.e. $L_0 = 38\,\mathrm{m}$ and vary by $L_1 = 20\,\mathrm{m}$. The water depth is $H = 1000\,\mathrm{m}$ throughout.

6. Conclusions

In the present study, we described three different numerical methods to solve the scattering problem of water waves from an ice floe modelled as a layer of mass loading material of random length L, where $L = L_0 + L_1\,\alpha$ and $\alpha \in [-1, 1]$ follows either a uniform or a transformed beta distribution. Two of the methods investigated belong to the family of generalised polynomial chaos (gPC) techniques. Specifically, these are a stochastic collocation method (SC) and a stochastic Galerkin method (SG). We also implemented a Monte Carlo technique (MC) for comparison.

Both gPC methods rely on a polynomial expansion of the relevant quantities in the random variable. While the SC method is non-intrusive and only post-processes results computed with the deterministic solver, the SG method generalises the equations characterising the system to account for the extra random dimension.

The gPC methods were shown to outperform MC significantly. Specifically, they exhibit exponential convergence, while MC converges only with the inverse square root of the sample size. As a result, the gPC methods achieve six digit accuracy within less than 3 s (usually less than 1 s), while MC reaches only comparably low accuracy after 60 s.

Compared to each other, the gPC methods show similar performance. Which method is faster depends on the length distribution considered. Specifically, we found that with $\alpha \sim \mathcal{U}$ the SG method is slightly faster, while with $\alpha \sim \mathcal{B}$ it is significantly slower than SC.

In contrast to the SG method, the derivation and implementation of the SC method is straightforward. Moreover, the SC method can be used to compute the moments of the evanescent amplitudes as well if required, and therefore does not have any disadvantage compared to the SG method which always calculates the complete probabilistic scattering matrix. In conclusion, the simplicity and superior performance of the SC method makes it more suitable for most applications.

We finally used the SC method to compute how the expected reflection coefficient depends on the wave period and floe thickness. This is an important result, as it suggests that the distribution of floe sizes present in a field of sea ice floes will be vitally important to the manner in which ocean waves are scattered.

The authors have generalised this study to floating elastic plates (not presented here).

The gPC framework can also be applied to non-linear problems and geometries with several random variables, although the latter case is a major challenge in the development of gPC which is an active field of research.

Appendix A. Scattering from the beam's edge

In this appendix we briefly discuss the procedure we follow to match the plane wave solutions on either side of the floe's edge.

The vertical modes ς_n and ζ_n defined in (13) and (14), respectively, are orthogonal with respect to the scalar product

$$\langle f_1, f_2 \rangle_z = \int_{-H}^{0} f_1(z)\, f_2(z)\, \mathrm{dz} \ , \tag{A.1}$$

that is

$$\langle \varsigma_m, \varsigma_n \rangle_z = \delta_{mn} \, \|\varsigma_m\| \tag{A.2}$$

$$\langle \zeta_m, \zeta_n \rangle_z = \delta_{mn} \, \|\zeta_m\| \tag{A.3}$$

where

$$\|\varsigma_m\| = \frac{\kappa_m \, H \, \mathrm{sech}^2(\kappa_m \, H) + \tanh(\kappa_m \, H)}{2 \, \kappa_m} \tag{A.4}$$

$$\|\zeta_m\| = \frac{k_m \, H \, \mathrm{sech}^2(k_m \, H) + \tanh(k_m \, H)}{2 \, k_m} \ . \tag{A.5}$$

We follow [26] and define an auxiliary function

$$u(z) = \partial_x \phi^-(x,z)|_{x=0} = \partial_x \phi^+(x,z)|_{x=0} \ , \tag{A.6}$$

thereby utilizing the condition of matching horizontal fluid velocities. By projecting on the respective vertical modes, we can express the amplitudes A_n^+ and B_n^- in terms of u:

$$A_n^+ = B_n^+ + \frac{\langle \zeta_n, u \rangle_z}{\mathrm{i} \, k_n \, \|\zeta_n\|} \ , \tag{A.7}$$

$$B_n^- = A_n^- - \frac{\langle \varsigma_n, u \rangle_z}{\mathrm{i} \, \kappa_n \, \|\varsigma_n\|} \ . \tag{A.8}$$

Matching the potentials

$$\phi^-(x,z) = \phi^+(x,z) \ , \qquad x = 0 \ , \tag{A.9}$$

and using (11), (12), (A.7), and (A.8), we obtain

$$2\,\mathrm{i}\,\kappa_l\,A_l^- - \sum_{n=0}^{N_\mathrm{match}} 2\,\mathrm{i}\,\frac{\kappa_l}{\|\varsigma_l\|}\,\langle\varsigma_l,\zeta_n\rangle_z\,B_n^+ = \sum_{n,m=0}^{N_\mathrm{match}} \Big(\delta_{ln}\,\delta_{nm} + \frac{\kappa_l}{\|\varsigma_l\|}\,\langle\varsigma_l,\zeta_n\rangle_z\,\frac{1}{k_n\,\|\zeta_n\|}\langle\zeta_n,\varsigma_m\rangle_z\Big)\,u_m\ , \tag{A.10}$$

where we have expanded $u(z) = \sum_{m=0}^{N_\mathrm{match}} u_m\,\varsigma_m(z)$. Note, that we use N_match instead of N_ζ, where $N_\mathrm{match} \gg N_\zeta$ so that the matching problem is solved with high accuracy. Later on we truncate the resulting matrices such that only N_ζ evanescent modes are taken into account for further computations.

Defining the $(N_\zeta+1)\times(N_\zeta+1)$ matrix $\underline{Z}$ with entries $\underline{e}_i^\mathrm{T}\cdot\underline{Z}\cdot\underline{e}_j = \langle\varsigma_i,\zeta_j\rangle_z$, as well as the vector $\underline{u} = (u_0,\ldots,u_{N_\zeta})^\mathrm{T}$, we can write (A.10) in matrix form as follows

$$\underline{u} = 2\,\mathrm{i}\,\Big(\underline{1} + \underline{K}^-\cdot(\underline{\zeta}^-)^{-1}\cdot\underline{Z}\cdot(\underline{K}^+)^{-1}\cdot(\underline{\zeta}^+)^{-1}\cdot\underline{Z}^\mathrm{T}\Big)^{-1} \cdot\Big(\underline{K}^-\cdot\underline{A}^- - \underline{K}^-\cdot(\underline{\zeta}^-)^{-1}\cdot\underline{Z}\cdot\underline{B}^+\Big)\ , \tag{A.11}$$

where $\underline{K}^+$, $\underline{K}^-$, $\underline{\zeta}^+$ and $\underline{\zeta}^-$ are diagonal matrices with the diagonal elements k_i, κ_i, $\|\zeta_i\|$, and $\|\varsigma_i\|$, respectively. In this notation, equations (A.7) and (A.8) become

$$\underline{A}^+ = \underline{B}^+ - \mathrm{i}\,(\underline{K}^+)^{-1}\cdot(\underline{\zeta}^+)^{-1}\cdot\underline{Z}^\mathrm{T}\cdot\underline{u} \tag{A.12}$$

$$\underline{B}^- = \underline{A}^- + \mathrm{i}\,(\underline{K}^-)^{-1}\cdot\underline{u}\ . \tag{A.13}$$

Comparing this to (19) we identify the reflection and transmission matrices

$$\underline{T}^- = 2\,(\underline{K}^+)^{-1}\cdot(\underline{\zeta}^+)^{-1}\cdot\underline{Z}^\mathrm{T}\cdot\Big(...\Big)^{-1}\cdot\underline{K}^- \tag{A.14}$$

$$\underline{R}^+ = \underline{1} - 2\,(\underline{K}^+)^{-1}\cdot(\underline{\zeta}^+)^{-1}\cdot\underline{Z}^\mathrm{T}\cdot\Big(...\Big)^{-1}\cdot\underline{K}^-\cdot(\underline{\zeta}^-)^{-1}\cdot\underline{Z} \tag{A.15}$$

$$\underline{R}^- = \underline{1} - 2\,(\underline{K}^-)^{-1}\Big(...\Big)^{-1}\cdot\underline{K}^- \tag{A.16}$$

$$\underline{T}^+ = 2\,(\underline{K}^-)^{-1}\Big(...\Big)^{-1}\cdot\underline{K}^-\cdot(\underline{\zeta}^-)^{-1}\cdot\underline{Z}\ , \tag{A.17}$$

where

$$\Big(...\Big)^{-1} = \Big(\underline{1} + \underline{K}^-\cdot(\underline{\zeta}^-)^{-1}\cdot\underline{Z}\cdot(\underline{K}^+)^{-1}\cdot(\underline{\zeta}^+)^{-1}\cdot\underline{Z}^\mathrm{T}\Big)^{-1}\ ,$$

as in equation (A.11).

For our analysis we solve the matching problem with $N_{\text{match}} = 100$ and then truncate the sizes of the resulting matrices such that only $N_\zeta = 5$ evanescent modes are considered. This ensures that the transmission coefficient T is computed with six digits of accuracy.

Acknowledgements

J.E.M.M. was supported by a University of Otago Postgraduate Scholarship. F.M. and V.A.S. were supported by the Office of Naval Research Departmental Research Initiative "Sea State and Boundary Layer Physics of the Emerging Arctic Ocean" (award N00014-131-0279), the EU FP7 grant (SPA-2013.1.1-06), and the University of Otago. We also thank Stuart Hawkins for interesting discussions during the KOZWaves conference, as well as the reviewers for their constructive comments. The source code necessary to reproduce the figures presented in this article is available from the authors upon request (jmosig@maths.otago.ac.nz).

References

[1] V. A. Squire, Synergies Between VLFS Hydroelasticity and Sea Ice Research, Int. J. Offshore Polar 18 (3) (2008) 1–13.

[2] E. Watanabe, T. Utsunomiya, C. M. Wang, Hydroelastic analysis of pontoon-type VLFS: a literature survey, Eng. Struct. 26 (2) (2004) 245–256. doi:10.1016/j.engstruct.2003.10.001.

[3] V. A. Squire, Of ocean waves and sea-ice revisited, Cold Reg. Sci. Technol. 49 (2) (2007) 110–133. doi:10.1016/j.coldregions.2007.04.007.

[4] M. Meylan, V. A. Squire, The response of ice floes to ocean waves, J. Geophys. Res. - Oceans 99 (C1) (1994) 891–900. doi:10.1029/93JC02695.

[5] I. V. Sturova, Oblique incidence of surface waves on an elastic plate, J. Appl. Mech. Tech. Phys. 40 (4) (1999) 604–610. doi:10.1007/BF02468434.

[6] A. I. Andrianov, A. J. Hermans, The influence of water depth on the hydroelastic response of a very large floating platform, Mar. Struct. 16 (5) (2003) 355–371. doi:10.1016/S0951-8339(03)00023-6.

[7] R. E. Taylor, Hydroelastic analysis of plates and some approximations, J. Eng. Math. 58 (1-4) (2006) 267–278. doi:10.1007/s10665-006-9121-7.

[8] T. D. Williams, V. A. Squire, Oblique scattering of plane flexuralgravity waves by heterogeneities in seaice, Philos. T. Roy. Soc. A 460 (2052) (2004) 3469–3497. doi:10.1098/rspa.2004.1363.

[9] L. G. Bennetts, N. R. T. Biggs, D. Porter, A multi-mode approximation to wave scattering by ice sheets of varying thickness, J. Fluid. Mech. 579 (2007) 413–443. doi:10.1017/S002211200700537X.

[10] M. J. A. Smith, M. H. Meylan, Wave scattering by an ice floe of variable thickness, Cold Reg. Sci. Technol. 67 (12) (2011) 24–30. doi:10.1016/j.coldregions.2011.03.003.

[11] M. H. Meylan, V. A. Squire, Response of a circular ice floe to ocean waves, J. Geophys. Res. - Oceans 101 (C4) (1996) 8869–8884. doi:10.1029/95JC03706.

[12] M. A. Peter, M. H. Meylan, H. Chung, Wave Scattering By a Circular Elastic Plate In Water of Finite Depth: A Closed Form Solution, Int. J. Offshore Polar Eng. 14 (02).

[13] F. Montiel, L. G. Bennetts, V. A. Squire, F. Bonnefoy, P. Ferrant, Hydroelastic response of floating elastic discs to regular waves. Part 2. Modal analysis, J. Fluid. Mech. 723 (2013) 629–652. doi:10.1017/jfm.2013.124.

[14] L. G. Bennetts, N. R. T. Biggs, D. Porter, Wave scattering by an axisymmetric ice floe of varying thickness, IMA J. Appl. Math. 74 (2) (2009) 273–295. doi:10.1093/imamat/hxn019.

[15] M. H. Meylan, Wave response of an ice floe of arbitrary geometry, J. Geophys. Res. - Oceans 107 (C1). doi:10.1029/2000JC000713.

[16] L. G. Bennetts, T. D. Williams, Wave scattering by ice floes and polynyas of arbitrary shape, J. Fluid. Mech. 662 (2010) 5–35. doi:10.1017/S0022112010004039.

[17] T. Toyota, C. Haas, T. Tamura, Size distribution and shape properties of relatively small sea-ice floes in the Antarctic marginal ice zone in late winter, Deep Sea Research Part II: Topical Studies in Oceanography 58 (910) (2011) 1182–1193. doi:10.1016/j.dsr2.2010.10.034.

[18] Z. Lu, D. Zhang, A Comparative Study on Uncertainty Quantification for Flow in Randomly Heterogeneous Media Using Monte Carlo Simulations and Conventional and KL-Based Moment-Equation Approaches, SIAM J. Sci. Comput. 26 (2) (2004) 558–577. doi:10.1137/S1064827503426826.

[19] D. Xiu, Numerical methods for stochastic computations: a spectral method approach, Princeton University Press, Princeton, N.J, 2010.

[20] M. Ganesh, S. C. Hawkins, Scattering by stochastic boundaries: hybrid low- and high-order quantification algorithms, ANZIAM J. 56 (0) (2016) 312–338, 00000. doi:10.0000/anziamj.v56i0.9313.

[21] X. Wan, G. E. Karniadakis, An adaptive multi-element generalized polynomial chaos method for stochastic differential equations, J. Comput. Phys. 209 (2) (2005) 617–642. doi:10.1016/j.jcp.2005.03.023.

[22] O. P. Le Matre, O. M. Knio, H. N. Najm, R. G. Ghanem, Uncertainty propagation using WienerHaar expansions, J. Comput. Phys. 197 (1) (2004) 28–57. doi:10.1016/j.jcp.2003.11.033.

[23] M. Weitz, J. B. Keller, Reflection of water waves from floating ice in water of finite depth, Commun. Pur. Appl. Math. 3 (3) (1950) 305–318.

[24] P. Wadhams, B. Holt, Waves in frazil and pancake ice and their detection in Seasat synthetic aperture radar imagery, J. Geophys. Res. - Oceans 96 (C5) (1991) 8835–8852. doi:10.1029/91JC00457.

[25] J. M. Gere, S. P. Timoshenko, Mechanics of Materials, Springer US, Boston, MA, 1991.

[26] T. D. Williams, R. Porter, The effect of submergence on the scattering by the interface between two semi-infinite sheets, J. Fluid. Struct. 25 (5) (2009) 777–793. doi:10.1016/j.jfluidstructs.2009.02.001.

[27] T. D. Williams, V. A. Squire, Scattering of flexuralgravity waves at the boundaries between three floating sheets with applications, J. Fluid Mech. 569 (2006) 113–140. doi:10.1017/S0022112006002552.

[28] C. M. Linton, H. Chung, Reflection and transmission at the ocean/sea-ice boundary, Wave Motion 38 (1) (2003) 43–52. doi:10.1016/S0165-2125(03)00003-9.

[29] C. Fox, V. A. Squire, On the oblique reflexion and transmission of ocean waves at shore fast sea ice, Philos. T. Roy. Soc. A 347 (1682) (1994) 185–218. doi:10.1098/rsta.1994.0044.

[30] F. Montiel, L. G. Bennetts, V. A. Squire, The transient response of floating elastic plates to wavemaker forcing in two dimensions, Journal of Fluids and Structures 28 (2012) 416–433. doi:10.1016/j.jfluidstructs.2011.10.007.

[31] L. G. Bennetts, V. A. Squire, On the calculation of an attenuation coefficient for transects of ice-covered ocean, Proc. R. Soc. A 468 (2137) (2012) 136–162. doi:10.1098/rspa.2011.0155.

[32] O. M. Knio, O. P. Le Maitre, Uncertainty propagation in CFD using polynomial chaos decomposition, Fluid Dyn. Res. 38 (9) (2006) 616–640.

[33] G. H. Golub, J. H. Welsch, Calculation of Gauss quadrature rules, Math. Comp. 23 (106) (1969) 221–230. doi:10.1090/S0025-5718-69-99647-1.

[34] A. L. Kohout, M. H. Meylan, An elastic plate model for wave attenuation and ice floe breaking in the marginal ice zone, J. Geophys. Res. 113 (C9) (2008) C09016. doi:10.1029/2007JC004434.

[35] D. Xiu, D. M. Tartakovsky, Numerical methods for differential equations in random domains, SIAM J. Sci. Comput. 28 (3) (2006) 1167–1185.